HHS Public Access

Author manuscript

J Burn Care Res. Author manuscript; available in PMC 2016 May 01.

Published in final edited form as:

J Burn Care Res. 2015 ; 36(3): e125–e135. doi:10.1097/BCR.0000000000000097.

Biphasic Presence of Fibrocytes in a Porcine Hypertrophic Scar Model

Taryn E. Travis, MD[†], **Matthew J. Mino, MD**[†], **Lauren T. Moffatt, PhD**[†], **Neil A. Mauskar, MD**[†], **Nicholas J. Prindeze, BS**[†], **Pejhman Ghassemi, PhD**[¶], **Jessica C. Ramella-Roman, PhD**[¶], **Marion H. Jordan, MD, FACS**[†], and **Jeffrey W. Shupp, MD**[†,¶]

[†]The Burn Center, Department of Surgery, MedStar Washington Hospital Center, MedStar Health Research Institute, Washington, DC, USA

[¶]Department of Biomedical Engineering, Catholic University of America, Washington, DC, USA

Abstract

Objective—The duroc pig has been described as a promising animal model for use in the study of human wound healing and scar formation. However little is known about the presence and chronology of the fibrocyte cell population in the healing process of these animals.

Methods—Wounds known to form scar were created on red duroc swine (3“ × 3”) with a dermatome to a total depth of either 0.06“ or 0.09”. These wounds were allowed to heal completely and were biopsied at scheduled time points during the healing process. Biopsies were formalin-fixed and paraffin embedded for immunohistochemical analysis. Porcine-reactive antibodies to CD-45 and procollagen-1 and a human-reactive antibody to LSP-1 were used to detect the presence of fibrocytes in immunohistochemistry an immunocytochemistry.

Results—Initial immunohistochemical studies showed evidence of a biphasic presence of fibrocytes. Pigs with 0.06“ deep wounds showed positive staining for CD-45 and LSP-1 within highly cellular areas at days 2 and 4 after wounding. Additional animals with 0.09” deep wounds showed positive staining within similar areas at days 56, 70, and 113 after wounding. There was no immunohistochemical evidence of fibrocytes in skin biopsies taken at days 14, 28, or 42. Procollagen-1 staining was diffuse in all samples. Cultured cells stained for CD-45, LSP-1, and procollagen-1 by immunocytochemistry.

Conclusions—These data confirm that fibrocytes are indeed present in this porcine model. We conclude that these cells are present after initial wounding and later during scar formation and remodeling. We believe that this is evidence of a biphasic presence of fibrocytes, first as an acute response to skin wounding followed by later involvement in the remodeling process, prompted by continued inflammation in a deep partial thickness wound.

Keywords

Fibrocyte; wound healing; hypertrophic scar; duroc pig

Corresponding Author: Jeffrey W. Shupp, MD The Burn Center 110 Irving Street, NW Suite 3B-55 Washington, DC 20010 202.877.7347 (v) 202.877.7302 (f) jeffrey.w.shupp@medstar.net.

Conflicts of Interest: None

Introduction

Fibrocytes, a fibroblast-like peripheral blood mononuclear cell population first described in 1994 [5], have been implicated in wound healing, scar formation, and fibrotic disease processes. Since then, numerous studies performed on human tissues [1, 5, 11, 16, 26, 28, 30, 33, 34] and in murine models [1, 5, 11, 15, 27, 28] have provided further information about these cells, such as their involvement in pulmonary hypertension [34] and their processes of differentiation [16]. Wound healing and hypertrophic scarring continue to provide challenges to clinicians and research in these areas often generates more knowledge along with more focused questions. The red duroc pig is emerging as one of the best available models of human skin physiology and pathophysiology. Despite the common use of the duroc model in studies of cutaneous injury and wound healing, as well as the increase in knowledge of the role of fibrocytes in associated processes, fibrocytes have not been described in swine. We sought to further our understanding of this cell type and determine if they are present in a red duroc porcine model of wound healing and scar.

Fibrocytes are bone-marrow derived cells that make up 0.1-0.5% of the peripheral white blood cell population [1, 3, 5]. In previous studies, these cells have been isolated from peripheral blood by separating the mononuclear cell layer from whole blood and allowing them to grow in culture [32], after which they are adherent and show a spindle-shaped morphology [1, 3, 5, 22]. Past work has shown that CD14+ precursors are promoted to differentiate into fibrocytes by IL-4 and IL-13 secreted from CD4+ Th2 cells and inhibited from differentiating to fibrocytes by IFN-γ, TNF-α, and IL-12 secreted from Th1 cells [14, 26].

Fibrocyte markers have been shown to include CD34, CD43, CD45, LSP-1, MHCII, collagen I, collagen III, CCR2 (murine), CCR7 (murine), CXCR4 (murine), vimentin, and fibronectin [5, 14, 22]. Cultured fibrocytes have been known to lose hematopoetic markers such as CD34 and CD45 and gain mesenchymal markers such as collagen and α-SMA between 2 and 4 weeks *in vitro* [15]. LSP-1 is a 52-kDa intracellular actin-binding protein that is absent in fibroblasts, but is expressed in lymphocytes, monocytes, and neutrophils [32]. Fibrocytes have been identified by the demonstration of procollagen-1 and LSP-1 coexpression [32], collagen I and CD45 coexpression [15], or collagen I and CD34 coexpression [5, 25].

After wounding, fibrocytes rapidly enter the site of injury from the peripheral blood [5, 32]. They are involved in the early stages of wound healing by migrating to the site of injury from the peripheral blood and attracting other inflammatory cells within hours to days [5, 15]. Fibrocytes produce proinflammatory cytokines TNF-α, IL-8, IL-6, IL-10, and MIP [8]. They also secrete extracellular matrix proteins and present antigens [1, 5, 17, 32]. Fibrocytes are believed to be involved in communicating with dermal fibroblasts for recruitment to the cause of wound healing and are thought to improve upon the pathogenic wound healing of diabetics in this way [15]. There is evidence that fibrocytes may promote angiogenesis in the proliferative stages of wound healing as well [14].

Fibrocytes are believed to be able to differentiate into myofibrocytes with expression of α-SMA and contractile capabilities when exposed to TGF-β, based on in vitro studies [1, 17, 22, 25]. Beyond wound contraction, fibrocytes are known to be involved in

scarring and fibrosis [23]. They have been implicated in lung fibrosis [21], asthma [25], atherosclerosis [19], hypertrophic scar [10, 29, 32, 33], and nephrogenic systemic fibrosis [4, 9]. Fibrocytes participate in remodeling by secreting matrix metalloproteinases.

The red duroc pig is currently a superior model to study human wound healing and hypertrophic scarring. Though duroc pigs are costly and labor-intensive as a wound healing model [36], they form fibroproliferative scars [35, 36] that have molecular markers similar to those seen in human wound healing [35-37], exhibit similar histologic appearance to human wounds [13, 36], and contain cell types seen in human wound healing [13, 36]. It is this great value of the duroc wound healing model combined with the promise of fibrocytes in the development of the field of fibroproliferative disease that led us to seek the presence of these cells in a porcine model of hypertrophic scarring.

Methods

Animal Model and Wound Creation

All animal work described was reviewed and approved by the MedStar Health Research Institute's Institutional Animal Care and Use Committee (IACUC). Juvenile castrated male Duroc swine (30-55kg) were received and handled according to facility standard operating procedures under an animal care and use program accredited by the Association for Assessment and Accreditation of Laboratory Animal Care International.

On the day of surgery, animals were anesthetized with a combination of ketamine and xylazine delivered intramuscularly. Animals were intubated, maintained on isoflurane, placed on a warming blanket, and ventilated while heart rate, peripheral oxygen saturation, and core body temperature were continuously monitored by trained research staff. The body hair was clipped and the skin was prepped with chlorhexidine gluconate scrub. For partial-thickness wounds, three 3 inch × 3 inch (7.6 cm × 7.6 cm) squares of skin were outlined and excised over the rib cage using a Zimmer dermatome (Zimmer, Ltd., Swindon, UK) at a total depth of 0.060 inches (0.030 in at two passes) (Figure 1A). For full thickness wounds, one 4 inch × 4 inch (10.16 cm × 10.16 cm) square was excised over the rib cage on each side, at a total depth of 0.090 inches (0.030 in at 3 passes) (Figure 1E). Punch biopsies were taken at baseline (pre-excision) and immediately post-excision. Punch biopsies were placed in formalin for subsequent histology (3 mm) or in Allprotect Tissue Reagent (Qiagen, Hilden, Germany) for subsequent RNA isolation. Biopsy sites were each closed with a simple interrupted 4-0 Prolene polypropylene suture (Ethicon, Somerville, NJ). Mepilex Ag dressings (Monlylke, Gothenburg, Sweden) were applied to wounds after biopsy closure. Animals were then fitted with custom-made 2-3 mm thick neoprene vests [20], which completely covered the applied dressings while allowing mobility of the animal. Buprenorphine and fentanyl were administered for pain control at the end of each surgical procedure. Animals with partial thickness wounds returned to the operating room every 2-3 days until day 14 post-wound creation for examinations, dressing changes, and biopsies. Animals with full-thickness wounds returned to the operating room every 7 days until day 113 post-wound creation for examinations, dressing changes, and biopsies. Digital photographs were taken at a fixed distance of 25 cm between camera and wound at each time point. Once scars began to form in animals with full thickness wounds, the Vancouver

Scar Scale was used to quantify and track scar progression [2]. The animals were examined in the animal housing facility at least twice daily to monitor animal health and to identify any signs of pain, wound infection, or distress.

Cell culture

At each wound time point, approximately 16 ml of peripheral blood was drawn into a heparinized cell preparation tube (BD, Franklin Lakes, NJ). Tubes were centrifuged at 1700 RCF for 25 minutes. The buffy coat was then pipetted into a sterile conical vial with PBS, and centrifuged again at 300 RCF for 15 minutes. The resulting cell pellet was resuspended in Dulbecco's modified Eagle's medium (DMEM) with L-glutamine (Thermo Fisher Scientific, Rockville, MD), pH 6.8-7.0, supplemented with 1.2 g/L of NaHCO3, 20% pig serum, 100 μ/ml penicillin (MP Biomedics, Solon, OH), and 100 mg/ml streptomycin (MP Biomedics, Solon, OH). Pig serum was isolated by collecting whole blood, allowing it to clot, and isolating the serum from collection vials after centrifugation. The DMEM-cell suspension was plated into 6 wells of a plastic 24-well plate and allowed to grow, with medium changes every 2 days.

After 10-14 days, cells were released from culture wells using trypsin-EDTA (Lonza, Walkersville, MD). Fibrocytes were separated from other PBMCs by immunodepletion as previously described by Tredget, *et al* [30, 32]. After immunodepletion of T-lymphocytes, B-lymphocytes, and monocytes, remaining cells were plated onto 8-chamber glass slides (Lab-Tek, Scotts Valley, CA) for immunocytochemistry.

Immunocytochemistry

Glass slides with fibrocyte growth were washed gently with PBS for 10 minutes. They were then fixed in 10% neutral buffered formalin for 10 minutes. After a 5 minute rinse with PBS, cells were permeabilized with a 10 minute wash in 0.025% Triton X-100. Slides were once again washed in PBS for 10 minutes, then blocked in 5% nonfat milk, 1% BSA, in PBS for 2 hours. After blocking, slides were incubated with monoclonal mouse anti-human LSP-1 IgG_1 (BD Biosciences, San Jose, CA), monoclonal mouse anti-pig CD45 IgM (Pierce, Rockford, IL), or monoclonal rat anti-pig procollagen-I IgG_1 (Abcam, Cambridge, UK) primary antibody diluted 1:100 in PBS-0.05% Tween-20 at 60°C for 2 ½ hours, then overnight at 4 °C. Controls were incubated in PBS-0.05% Tween-20 only. After overnight incubation with primary antibody, slides were washed for 10 minutes in 0.025% Triton-X-100. Endogenous peroxidase activity was quenched with 15 minute incubation in 0.3% H_2O_2. Goat polyclonal anti-mouse IgG+IgM-HRP secondary antibody (Abcam, Cambridge, UK) or goat polyclonal anti-rat IgG-HRP (Abcam, Cambridge, UK) diluted 1:100 in PBS-1% BSA was applied for 1 hour at room temperature. Controls were incubated in the anti-rat secondary antibody. Slides were then developed with DAB peroxidase substrate (Vector Laboratories, Burlingame, CA) for 10 minutes before being mounted and viewed under light microscopy.

Immunohistochemistry

Punch biopsies were fixed in 10% formalin and embedded in paraffin. Paraffin blocks were sectioned at a thickness of 4 μm and baked at 60°C. After cooling, slides were

deparaffinized and rehydrated with PBS. Antigen retrieval was performed in Tris-EDTA buffer at 95-100 °C for 20 minutes. Slides were then cooled for 5 minutes in running cold water. Slides were washed in 0.025% Triton X-100 for 5 minutes twice. Slides were blocked in 5% nonfat milk 1% BSA in PBS for 2 hours. After blocking, slides were incubated with monoclonal mouse anti-human LSP-1 IgG_1 (BD Biosciences, San Jose, CA), monoclonal mouse anti-pig CD45 IgM (Pierce, Rockford, IL), or monoclonal rat anti-pig procollagen-I IgG_1 (Abcam, Cambridge, UK) primary antibody diluted 1:100 in PBS-0.05% Tween-20 at room temperature overnight. Controls were incubated in PBS-0.05% Tween-20 only. After overnight incubation with primary antibody, slides were rinsed with 0.025% Triton-X-100 for 5 minutes twice. Endogenous peroxidase activity was quenched with 15 minute incubation in 0.3% H_2O_2. Goat polyclonal anti-mouse IgG+IgM-HRP (Abcam, Cambridge, UK) or goat polyclonal anti-rat IgG-HRP (Abcam, Cambridge, UK) secondary antibody was applied for 1 hour at room temperature. Slides were rinsed with PBS for 5 minutes three times, then developed with DAB peroxidase substrate (Vector Laboratories, Burlingame, CA) for 10 minutes. After 5 minute rinse with running tap water, slides were counterstained with hematoxylin, cleared, and mounted, then viewed with a Zeiss Axioimager microscope and brightfield color camera (Carl Zeiss, Oberkochen, Ger).

Immunofluorescence

Punch biopsies were fixed in 10% formalin and embedded in paraffin. Paraffin blocks were sectioned at a thickness of 4 μm and baked at 60°C. After cooling, slides were deparaffinized and rehydrated with PBS. Antigen retrieval was performed in Tris-EDTA buffer at 95-100 °C for 20 minutes. Slides were then cooled for 5 minutes in running cold water. Slides were washed in 0.025% Triton X-100 for 5 minutes twice. Slides were blocked in 5% nonfat milk 1% BSA in PBS for 2 hours. After blocking, slides were incubated with monoclonal mouse anti-human LSP-1 IgG_1 (BD Biosciences, San Jose, CA) primary antibody diluted 1:100 in PBS-0.05% Tween-20 at room temperature overnight. Controls were incubated in PBS-0.05% Tween-20 only. After overnight incubation with primary antibody, slides were rinsed with 0.025% Triton-X-100 for 5 minutes twice. Polyclonal goat anti-mouse IgG-FITC conjugated secondary antibody (EMD Millipore, Billerica, MA) diluted 1:100 was then applied and slides were incubated at room temperature for one hour. Slides were rinsed with PBS for 5 minutes three times, then blocked again in 5% nonfat milk 1% BSA in PBS for 2 hours. After the second blocking step, slides were incubated with monoclonal rat anti-pig procollagen-I IgG_1 (Abcam, Cambridge, UK) primary antibody diluted 1:100 in PBS-0.05% Tween-20 at room temperature overnight. Controls were incubated in PBS-0.05% Tween-20 only. After overnight incubation with the second primary antibody, slides were rinsed with 0.025% Triton-X-100 for 5 minutes twice. Polyclonal goat anti-rat IgG-rhodamine conjugated secondary antibody (EMD Millipore, Billerica, MA) diluted 1:100 was then applied and slides were incubated at room temperature for one hour. Slides were rinsed with PBS for 5 minutes three times, then stained with DAPI (Santa Cruz Biotechnology, Dallas, TX) for 10 minutes. Slides were then viewed with a Zeiss Axioimager microscope, and multichannel black and white camera equipped with fluorescence filters (Carl Zeiss, Oberkochen, Ger).

Hematoxylin and eosin staining

Punch biopsies were fixed in 10% formalin and embedded in paraffin. Paraffin blocks were sectioned at a thickness of 4 μm and baked at 60°C. After cooling, slides were deparaffinized and rehydrated with PBS. Slides were then stained with hematoxylin and eosin, before dehydrating, clearing, and mounting. Slides were viewed with a Zeiss Axioimager microscope and brightfield color camera (Carl Zeiss, Oberkochen, Ger).

RNA isolation and gene expression analysis

RNA was extracted from All-Protect-preserved biopsies using the RNA Animal Tissue (RNeasy Fibrous Tissue Kit) (Qiagen Inc., Valencia, CA). Thawed samples were first removed from reagent and homogenized using the TissueLyser (Qiagen Inc., Valencia, CA) bead homogenizer. The samples were shaken at 40Hz in a sonicator for 5 min, then immediately cooled on ice for another 5 min, followed by another round of shaking at 40Hz for 5 min again. Homogenates were then processed per kit protocol. Resulting DNA and protein samples were preserved for later use. RNA sample quality and quantity were obtained using a Bioanalyzer RNA 6000 NanoKit (Agilent Technologies, Inc. 2001, 2003-2006, Cat: G2938-90034) and recorded.

RNA samples were diluted to 1 ng/μl and added to BioRad SYBR Green master mix (BioRad Laboratories Inc, Hercules, CA) with gene-specific primers and reverse transcriptase in 96 well plates. As a reference gene, levels of glyceraldehyde 3-phosphate dehydrogenase (GAPDH) were quantified in parallel with target genes. The following sequences (Integrated DNA Technologies, Coralville, IA) were utilized in PCR: Pig GAPDH, forward 5’- CTCAACGACCACTTCGTCAA -3’ and reverse 5’- TCCAGGGGCTCTTACTCCTT -3’; Pig COL1a, forward 5’- ACCTCAAGATGTGCCACTCC -3’ and reverse 5’- CCTGTCTCCATGTTGCAGAA -3’ [35].

Samples were loaded in a BioRad CFX96 RT system C1000 Thermal cycler (BioRad Laboratories Inc, Hercules, CA) and cycled as follows: step 1—50° C for 10 min, step2—95° C for 5 min, step3—95° C for 10 sec, step 4—60° C for 30 sec (repeat step 2-4 for 39 cycles) followed by 95° C for 1 min, step 5—55° C for 1 min. The ΔCt method was used in analyzing the resulting raw gene expression data. Briefly, the relative gene expression of the genes was calculated as ΔCt sample = (Ct sample gene) - (Ct sample reference gene) and ΔCt control = (Ct control gene) - (Ct reference gene). The fold regulation was then calculated as $2^{-[\Delta Ctsample-\Delta Ctcontrol]}$, where control was represented by samples collected at day 0 before any intervention.

Additionally, the transcript of secretory products of fibrocytes were quantified in a subset of scar samples (All-Protect-preserved biopsies from days 70, 77, 84, 90, and 99) using a multiplex real time RT-PCR system (SABiosciences, Qiagen, Valencia, CA). Genes of interest examined were TGFβ1, TGFβ3, COL1A2, MMP9, and TNFα [24]. Briefly, RNA was isolated and handled as above, but subsequently first strand cDNA synthesis was carried out using 100 ng of total RNA in an RT2 first strand kit (SABiosciences, Qiagen, Valencia, CA), according to the manufacturer's instructions.

Plates with wells containing gene specific primers and RT2 real-time SyBR Green/ROX PCR mix were purchased from SABiosciences and used according to the manufacturer's instructions for gene expression analysis. Assays were performed on an ABI Prism 7500Fast PCR system (Applied Biosystems, Foster City, CA). A set of five reference genes was included in the analysis for each sample and used for normalization. The ΔΔ Ct method was used in analyzing the resulting raw gene expression data as described above. Graphs and statistical analysis were performed using Prism GraphPad 6.0 (GraphPad Software, La Jolla, CA). Statistical significance was set at $p<0.05$.

Results

Wound characteristics

Partial thickness wounds were created at a total dermatome depth of 0.06 inches (1.5 mm) and with an area of 3 inches by 3 inches (Figure 1A, 2D). These wounds were generally reepithelialized by day 7 and healed without raised, firm scars (Figure 1B-D). Healed wounds on cross section showed dermal thicknesses slightly larger than that of normal uninjured skin (Figure 2A, 2B).

Full thickness wounds were created at a total dermatome depth of 0.09 inches (2.3 mm) and with an area of 4 inches by 4 inches (Figure 1E, 2D), These wounds were generally reepithelialized between days 30 and 40 and healed with a contracted, raised, firm scar (Fig 1E-I). Healed wounds on cross section showed dermal thickness considerably larger than that of normal uninjured skin (Figure 2A, 2C). As scars formed, they were evaluated using the Vancouver Scar Scale, with scores between 7 and 9, and showing a peak average value of 9±1 at day 84 after wounding. This full thickness wound creation approach served as our injury standard to create hypertrophic scar.

Cell culture and immunocytochemistry

Cells were isolated from the whole blood of wounded pigs and grown on culture plates after separation of the peripheral blood mononuclear cell layer. The population of cells that resulted from 10-14 days of growth were spindle-shaped and adherent (Figure 3). Immunodepletion of this population with anti-CD2, anti-CD14, and anti-CD19 immunomagnetic beads as previously described [30, 32] left a population of cells presumed to be fibrocytes, which were then grown on glass chamber slides. These slides were subjected to immunocytochemistry and showed positive staining for LSP-1, CD-45, and procollagen-1 (Figure 4).

Immunohistochemistry

Formalin-fixed biopsies were sectioned and subjected to immunohistochemistry. Procollagen-1 staining was ubiquitous in biopsies from all time points (Figure 5C, 5F). Both CD-45 and LSP-1 staining were seen biphasically. CD-45 and LSP-1 were absent in biopsies immediately prior to and immediately following wound creation, but were present at days 2 and 4 after wound creation (Figure 5A, 5B). There was an absence of staining for CD-45 and LSP-1 in samples taken at days 7, 9, 11, 14, 28, 35, and 42 after wound creation

(Figure 5G, 5H). Staining was evident again in samples taken at days 56, 70, and 113 after wound creation (Figure 5D, 5E). Control samples showed no staining (Figure 5I).

Immunofluorescence

Formalin-fixed biopsies were sectioned and subjected to immunofluorescence with DAPI, FITC, and CY3 filters. LSP-1 and procollagen-1 were colocalized in samples at days 2 and 4 after wound creation (Figure 6A) and again at days 56, 70, and 113 after wound creation (Figure 6B, 6C). Colocalization was not seen in samples taken at days 7, 9, 11, 14, 28, 35, and 42 after wound creation. Red blood cells showed autofluorescence and were discriminated from fibrocytes by the presence of a DAPI-positive nucleus (Figure 6A, 6E). Control images lacking primary antibody to either procollagen-1 or LSP-1 showed a lack of their respective color's staining.

RNA isolation and fibrocyte marker expression

RNA was isolated from biopsy samples taken from full thickness wounds during the process of wound healing and scar formation. Real-time RT-PCR analysis of these specimens showed an upregulation of COL1A1 at all timepoints examined, with highest peaks at days 49 and 56 after wound creation, compared to levels present in biopsies taken just prior to wound creation (Figure 7). RNA was isolated from two separate biopsies for days 0, 7, 21, 35, 49, 56, and 70, and from 4 separate biopsies for days 14, 28, and 43, determined by available stored samples. At day 7, COL1A1 was upregulated over 6-fold. This increased to almost 22-fold by day 43, and peaked at almost 179-fold on day 49. COL1A1 expression remained high at a 171-fold increase over baseline on day 56, and then trended downward to 33-fold on day 70 (Figure 7). There was a statistically significant difference between ΔCt sample and ΔCt control for COL1A1 expression starting at day 7 post-wounding ($p<0.005$).

RNA was isolated from biopsy samples taken from full thickness wounds at 5 time points of late scar formation during which our histological results indicated the presence of fibrocytes: days 70, 77, 84, 91, and 99 after full-thickness wound creation. Multiplex real-time RT-PCR of these specimens showed an upregulation of COL1A2, MMP9, TGFβ1, TGFβ3, and TNFα at all timepoints examined, with highest peaks at day 70 for MMP-9 with a 29-fold change from baseline biopsies and at day 99 for TNF-α and COL1A2 with 36-and 30-fold changes from baseline biopsies, respectively (Figure 8). TGFβ1 was most up regulated in these samples at day 99 with a 20-fold change from baseline as was TGFβ3, with a 14-fold increase from baseline uninjured skin biopsies.

Discussion

Fibrocytes are a specialized group of cells still incompletely understood, but overwhelmingly believed to be important in wound healing, fibrosis, and hypertrophic scarring. Originally described in 1994 [5], fibrocytes have been investigated in human tissues [1, 5, 11, 16, 26, 28, 30, 33, 34] and in murine experimental models [1, 5, 6, 11, 15, 28], but have not been identified in a porcine model of wound healing. The data presented in this study demonstrate the existence of fibrocytes in the red duroc pig and suggest fibrocyte involvement in inflammation as well as porcine wound remodeling and scar formation.

Prior studies of fibrocytes have shown them to be spindle-shaped when grown in culture [1, 3, 5, 22]. The cells that we isolated from the peripheral blood mononuclear cell layer of red duroc swine whole blood assumed this same shape and structure. Tredget *et al* have separated human fibrocytes from a population of peripheral blood mononuclear cells by the use of immunomagnetic beads [30, 32]. In this study, the same procedure was applied to the described population of porcine peripheral mononuclear blood cells to separate monocytes, T cells, and B cells from presumed fibrocytes. Subjected to immunocytochemistry, these isolated cells showed positive staining for LSP-1, CD45, and procollagen-1. Positivity of these markers in cells cultured from the peripheral blood mononuclear cell layer, separated from other PBMCs by immunodepletion, confirmed fibrocyte identity. With the knowledge that fibrocytes existed in the peripheral blood of red duroc pigs, we sought to identify them in the biopsy samples taken from the healing wounds and developing scars of these animals.

The biopsies examined using immunohistochemistry came from red durocs with wounds created at different sizes and depths. Swine with 3 inch by 3 inch wide and 0.06 inch deep wounds were biopsied every 2 days until healing at 2 weeks, and were the source of biopsies tested for the early presence of fibrocytes until day 14. Our partial thickness wounds reliably heal within 14 days and do not typically result in raised scar [18]. These wounds are well known to our lab to produce a model of normal partial-thickness wound healing, and were interesting to us for the purpose of demonstrating fibrocytes in a model that did not ultimately exhibit hypertrophic healing. Swine with 4 inch by 4 inch wide and 0.09 inch deep wounds were biopsied every 7 days until day 113, and were the source of biopsies tested for fibrocytes from day 7 onward. In this model, full thickness wounds generally heal within 30-40 days and then go through a process of fibroproliferative scar maturation. We were interested in the presence of fibrocytes beyond the early healing process that we see in our partial-thickness wounds and sought to demonstrate their presence in scar as well.

Fibrocytes in tissue have been previously identified by immunohistochemical staining for different combinations of LSP-1, CD-45, and procollagen-1 [5, 15, 25, 32]. The histology data presented here also showed evidence of fibrocytes by staining for these markers. Similar collections of cells in examined biopsies stained for CD-45 and LSP-1 at coincident time points; early in wound healing at days 2-4 and again later from day 56 onward.

It has been shown previously that fibrocytes migrate to the site of injury within hours to days [5, 15]. The first group of fibrocytes was immunohistochemically evident in the biopsies in this experiment at days 2 and 4, which supports the notion that they are early actors in inflammation and wound healing, presenting antigens, secreting chemokines, and recruiting other inflammatory cells [1, 5, 8, 15, 17, 32]. The lack of fibrocyte staining seen between these early biopsies and those starting at day 56 may indicate the proliferative period of wound healing where fibrocytes may be less active, between the acute inflammatory stage and the later remodeling stage.

We believe the second peak in IHC staining for fibrocytes suggests their involvement in the wound remodeling and scar formation process. It is known that fibrocytes secrete collagen-I [24], and here we sought to demonstrate transcript-level evidence of fibrocytes in our porcine model. Real time RT-PCR showed an upregulation of COL1A1 around day 56 after

wounding. When taken together with the histological evidence of fibrocytes around the same time in the healing process, this mRNA level data provides additional support confirming fibrocyte presence. Collagen levels tend to increase in scars and fibrotic processes. Based on evidence from our work and previous studies, it is reasonable to believe that fibrocytes may be involved in this process. Fibrocyte recruitment was shown to be directly correlated with collagen production in pulmonary fibrosis [21], and COL1A1 mRNA levels increased from month 2-7 in a human to mouse xenograft hypertrophic scar model [29]. Similarly, increased levels of COL1A1 mRNA coincident with detectable fibrocytes in scar biopsies were shown.

Along with collagen I, fibrocytes are known to have many other secretory products, including growth factors, colony stimulating factors, additional collagens, and interleukins [1, 7, 24]. We identified several that were of interest related to scar formation and remodeling and evaluated their expression in samples of late scar compared to uninjured skin. TGFβ is expressed widely and involved in many cell-signaling processes, but is of particular interest in the field of wound healing and scar formation for its association with fibrosis and worsened clinical scarring [12]. TGFβ1 and 3 were both upregulated moderately, with highest levels seen in samples from day 99. MMP9 is well-known for its involvement in matrix degradation and remodeling, and its spike in expression at day 70 in our studies, coincident with histological fibrocyte presence, may point to a process of concurrent scar remodeling. TNFα is generally seen in wound healing in the first 12-24 hours after injury [31], not unlike the very early presence of fibrocytes after injury. In data from late scar, there was an upregulation of TNFα compared to baseline, with a considerable increase at day 99. TNFα has also been known to increase ECM deposition and counteract MMPs [24], thus the peak at day 99, could be in response to the sharp upregulation of MMP9 at day 70, potentially related to fibrocyte presence. The proliferative phase of wound healing is generally believed to be a time when these markers are highly expressed. It is plausible that collagen, TGFβ, and others are even further upregulated during the proliferative time period as compared to the remodeling stage, however the remodeling stage was of particular interest in this study due to its correlation with fibrocyte presence. These are complex pathway interactions that will require future study.

Additional molecular work is needed; specifically, examination of CD45 and LSP-1 mRNA in order to buttress the results seen in immunohistochemical staining. At this time, these genes have not been sequenced for swine and have poor homology with other species, making primer design technically difficult. Only biopsies from the 4 inch by 4 inch wide and 0.09 inch deep wounds, sampled weekly from day 7 to 113 were available for RNA isolation and real-time RT-PCR. It is possible that a similar upregulation of COL1A1 mRNA was missed by not having biopsies to test from the first 7 days after wounding.

This study demonstrates the presence of fibrocytes in peripheral blood of wounded duroc pigs, strengthening this model for future studies of wound healing and scar formation. Additionally, a late presence of fibrocytes in evolving scar suggests their secondary function in wound remodeling.

Acknowledgments

We would like to thank Dr. Edward Tredget and his staff for their guidance on the isolation of fibrocytes. We thank Rachel Truhan-Ortiz and Daniel Jo for their assistance with RNA isolation and PCR.

Acknowledgments

Funding: NIH R15 EB 013439

References

1. Abe R, Donnelly SC, Peng T, et al. Peripheral Blood Fibrocytes: Differentiation Pathway and Migration to Wound Sites. J Immunol. 2001; 166:7556–62. [PubMed: 11390511]
2. Baryza MJ, Baryza GA. The Vancouver Scar Scale: An Administration Tool and Its Interrater Reliability. J Burn Care Rehabil. 1995; 16:535–8. [PubMed: 8537427]
3. Bellini A, Mattoli S. The Role of the Fibrocyte, a Bone Marrow-Derived Mesenchymal Progenitor, in Reactive and Reparative Fibroses. Lab Invest. 2007; 87:858–70. [PubMed: 17607298]
4. Bucala R. Circulating Fibrocytes: Cellular Basis for Nsf. J Am Coll Radiol. 2008; 5:36–9. [PubMed: 18180007]
5. Bucala R, Spiegel LA, Chesney J, et al. Circulating Fibrocytes Define a New Leukocyte Subpopulation That Mediates Tissue Repair. Mol Med. 1994; 1:71–81. [PubMed: 8790603]
6. Chesney J, Bacher M, Bender A, et al. The Peripheral Blood Fibrocyte Is a Potent Antigen-Presenting Cell Capable of Priming Naive T Cells in Situ. Proc Natl Acad Sci U S A. 1997; 94:6307–12. [PubMed: 9177213]
7. Chesney J, Bucala R. Peripheral Blood Fibrocytes: Mesenchymal Precursor Cells and the Pathogenesis of Fibrosis. Curr Rheumatol Rep. 2000; 2:501–5. [PubMed: 11123104]
8. Chesney J, Metz C, Stavitsky AB, et al. Regulated Production of Type I Collagen and Inflammatory Cytokines by Peripheral Blood Fibrocytes. J Immunol. 1998; 160:419–25. [PubMed: 9551999]
9. Cowper SE, Bucala R. Nephrogenic Fibrosing Dermopathy: Suspect Identified, Motive Unclear. Am J Dermatopathol. 2003; 25:358. [PubMed: 12876500]
10. Curran TA, Ghahary A. Evidence of a Role for Fibrocyte and Keratinocyte-Like Cells in the Formation of Hypertrophic Scars. J Burn Care Res. 2012
11. Ekert JE, Murray LA, Das AM, et al. Chemokine (C-C Motif) Ligand 2 Mediates Direct and Indirect Fibrotic Responses in Human and Murine Cultured Fibrocytes. Fibrogenesis Tissue Repair. 2011; 4:23. [PubMed: 22011363]
12. Gabriel VA. Transforming Growth Factor-Beta and Angiotensin in Fibrosis and Burn Injuries. J Burn Care Res. 2009; 30:471–81. [PubMed: 19349880]
13. Harunari N, Zhu KQ, Armendariz RT, et al. Histology of the Thick Scar on the Female, Red Duroc Pig: Final Similarities to Human Hypertrophic Scar. Burns. 2006; 32:669–77. [PubMed: 16905264]
14. Herzog EL, Bucala R. Fibrocytes in Health and Disease. Exp Hematol. 2010; 38:548–56. [PubMed: 20303382]
15. Kao HK, Chen B, Murphy GF, et al. Peripheral Blood Fibrocytes: Enhancement of Wound Healing by Cell Proliferation, Re-Epithelialization, Contraction, and Angiogenesis. Ann Surg. 2011; 254:1066–74. [PubMed: 21832942]
16. Maharjan AS, Pilling D, Gomer RH. High and Low Molecular Weight Hyaluronic Acid Differentially Regulate Human Fibrocyte Differentiation. PLoS One. 2011; 6:e26078. [PubMed: 22022512]
17. Mattoli S, Bellini A, Schmidt M. The Role of a Human Hematopoietic Mesenchymal Progenitor in Wound Healing and Fibrotic Diseases and Implications for Therapy. Curr Stem Cell Res Ther. 2009; 4:266–80. [PubMed: 19500063]
18. Mauskar NA, Sood S, Travis TE, et al. Donor Site Healing Dynamics: Molecular, Histological, and Noninvasive Imaging Assessment in a Porcine Model. J Burn Care Res. 2013; 34:549–62. [PubMed: 23511287]

19. Medbury HJ, Tarran SL, Guiffre AK, et al. Monocytes Contribute to the Atherosclerotic Cap by Transformation into Fibrocytes. Int Angiol. 2008; 27:114–23. [PubMed: 18427397]
20. Mino MJ, Mauskar NA, Matt SE, et al. A Fitted Neoprene Garment to Cover Dressings in Swine Models. Lab Anim (NY). 2012; 42:23–5. [PubMed: 23246889]
21. Phillips RJ, Burdick MD, Hong K, et al. Circulating Fibrocytes Traffic to the Lungs in Response to Cxcl12 and Mediate Fibrosis. J Clin Invest. 2004; 114:438–46. [PubMed: 15286810]
22. Pilling D, Fan T, Huang D, et al. Identification of Markers That Distinguish Monocyte-Derived Fibrocytes from Monocytes, Macrophages, and Fibroblasts. PLoS One. 2009; 4:e7475. [PubMed: 19834619]
23. Quan TE, Cowper SE, Bucala R. The Role of Circulating Fibrocytes in Fibrosis. Curr Rheumatol Rep. 2006; 8:145–50. [PubMed: 16569374]
24. Quan TE, Cowper S, Wu SP, et al. Circulating Fibrocytes: Collagen-Secreting Cells of the Peripheral Blood. Int J Biochem Cell Biol. 2004; 36:598–606. [PubMed: 15010326]
25. Schmidt M, Sun G, Stacey MA, et al. Identification of Circulating Fibrocytes as Precursors of Bronchial Myofibroblasts in Asthma. J Immunol. 2003; 171:380–9. [PubMed: 12817021]
26. Shao DD, Suresh R, Vakil V, et al. Pivotal Advance: Th-1 Cytokines Inhibit, and Th-2 Cytokines Promote Fibrocyte Differentiation. J Leukoc Biol. 2008; 83:1323–33. [PubMed: 18332234]
27. Thevenot PT, Baker DW, Weng H, et al. The Pivotal Role of Fibrocytes and Mast Cells in Mediating Fibrotic Reactions to Biomaterials. Biomaterials. 2011; 32:8394–403. [PubMed: 21864899]
28. Vannella KM, McMillan TR, Charbeneau RP, et al. Cysteinyl Leukotrienes Are Autocrine and Paracrine Regulators of Fibrocyte Function. J Immunol. 2007; 179:7883–90. [PubMed: 18025235]
29. Wang J, Ding J, Jiao H, et al. Human Hypertrophic Scar-Like Nude Mouse Model: Characterization of the Molecular and Cellular Biology of the Scar Process. Wound Repair Regen. 2011; 19:274–85. [PubMed: 21362096]
30. Wang JF, Jiao H, Stewart TL, et al. Fibrocytes from Burn Patients Regulate the Activities of Fibroblasts. Wound Repair Regen. 2007; 15:113–21. [PubMed: 17244327]
31. Xu F, Zhang C, Graves DT. Abnormal Cell Responses and Role of Tnf-Alpha in Impaired Diabetic Wound Healing. Biomed Res Int. 2013; 2013:754802. [PubMed: 23484152]
32. Yang L, Scott PG, Dodd C, et al. Identification of Fibrocytes in Postburn Hypertrophic Scar. Wound Repair Regen. 2005; 13:398–404. [PubMed: 16008729]
33. Yang L, Scott PG, Giuffre J, et al. Peripheral Blood Fibrocytes from Burn Patients: Identification and Quantification of Fibrocytes in Adherent Cells Cultured from Peripheral Blood Mononuclear Cells. Lab Invest. 2002; 82:1183–92. [PubMed: 12218079]
34. Yeager ME, Nguyen CM, Belchenko DD, et al. Circulating Fibrocytes Are Increased in Children and Young Adults with Pulmonary Hypertension. Eur Respir J. 2012; 39:104–11. [PubMed: 21700605]
35. Zhu KQ, Carrougher GJ, Couture OP, et al. Expression of Collagen Genes in the Cones of Skin in the Duroc/Yorkshire Porcine Model of Fibroproliferative Scarring. J Burn Care Res. 2008; 29:815–27. [PubMed: 18695616]
36. Zhu KQ, Carrougher GJ, Gibran NS, et al. Review of the Female Duroc/Yorkshire Pig Model of Human Fibroproliferative Scarring. Wound Repair Regen. 2007; 15(Suppl 1):S32–9. [PubMed: 17727465]
37. Zhu KQ, Engrav LH, Tamura RN, et al. Further Similarities between Cutaneous Scarring in the Female, Red Duroc Pig and Human Hypertrophic Scarring. Burns. 2004; 30:518–30. [PubMed: 15302416]

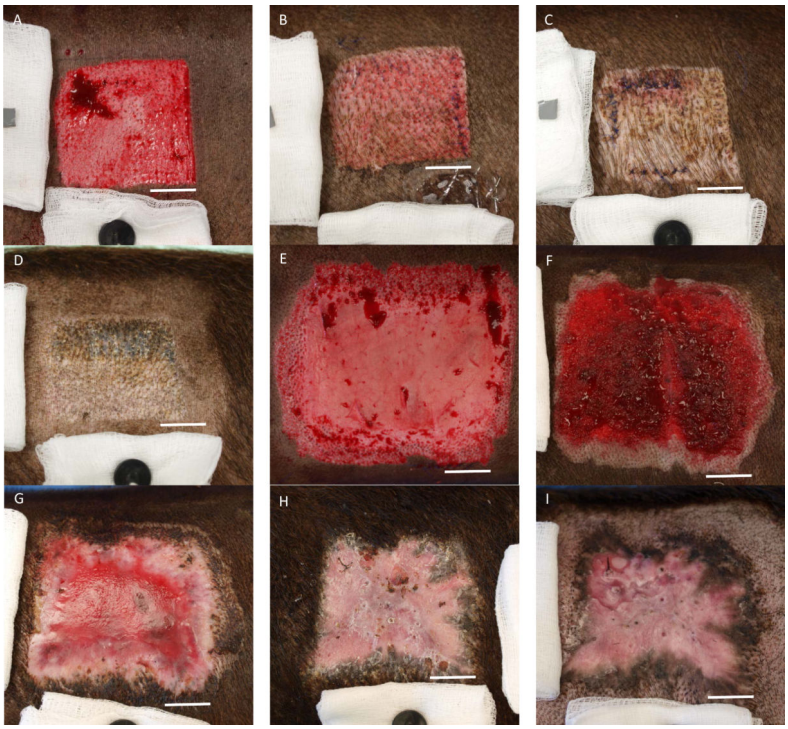

Figure 1.

Operating room photographs of partial thickness (A-D) and full thickness (E-I) wounds during the course of healing. Partial thickness wounds were created with dimensions of approximately 3in by 3in (7.6cm by 7.6cm) and a total dermatome depth of 0.06in (1.5mm) as shown in image A. The following images were taken at 7 (B), 14 (C), and 44 (D) days following wounding. Full thickness wounds were created with dimensions of approximately 4in by 4in (10.2cm by 10.2cm) and a total dermatome depth of 0.09in (2.3mm) as shown in image E. The following images were taken at 7 (F), 14 (G), 42 (H), and 70 (I) days after wounding. All photographs were taken at a distance of 25cm from the wound. Scale bar represents approximately 1 inch or 2.5cm.

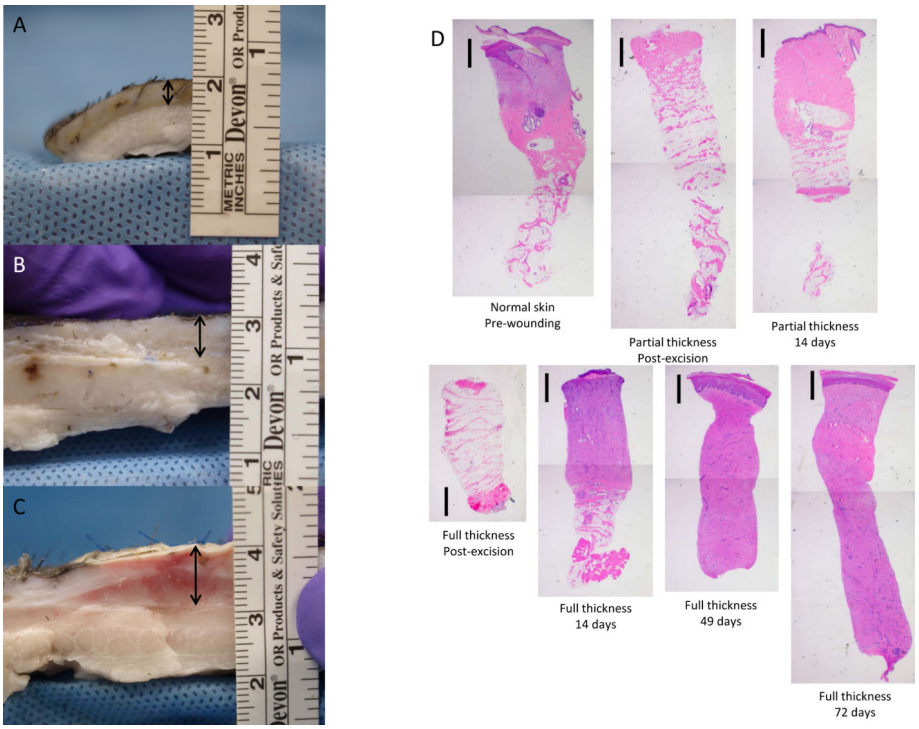

Figure 2.

Photographic representation of gross-specimen porcine skin and scar cut on cross section (A-C). Normal uninjured duroc skin seen in image A. Healed partial-thickness wound seen in image B. Healed full-thickness wound seen in image C. Section D is made up of photomicrographs of H&E-stained biopsy sections at different wound-excision depths and times in the healing process. In A-C, rulers are shown for scale and arrow represents approximate epidermal-dermal thickness. In D, scale bar represents 1mm.

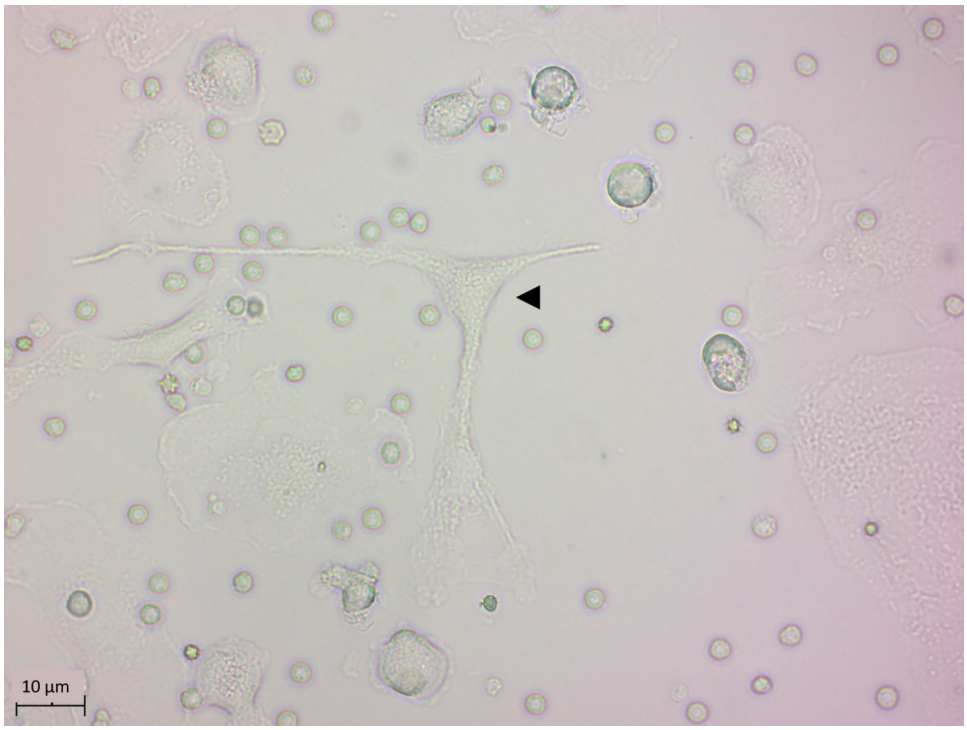

Figure 3.
Photomicrograph of porcine peripheral blood mononuclear cells in culture, with arrowhead pointing to a typical adherent, spindle-shaped fibrocyte. 400x magnification.

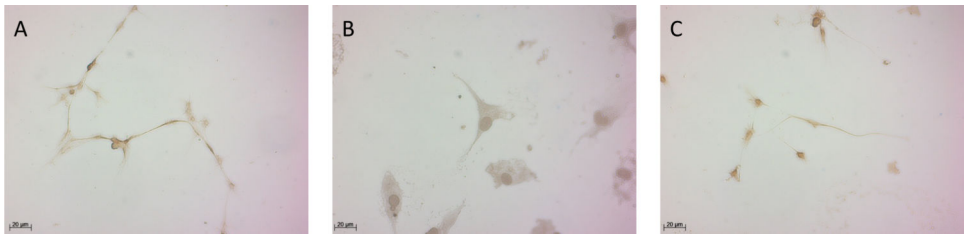

Figure 4.

Photomicrograph of fibrocytes immunocytochemically stained for A) LSP-1, B) CD-45, and C) procollagen-1. Control slides showed no staining (data not shown). 400x magnification.

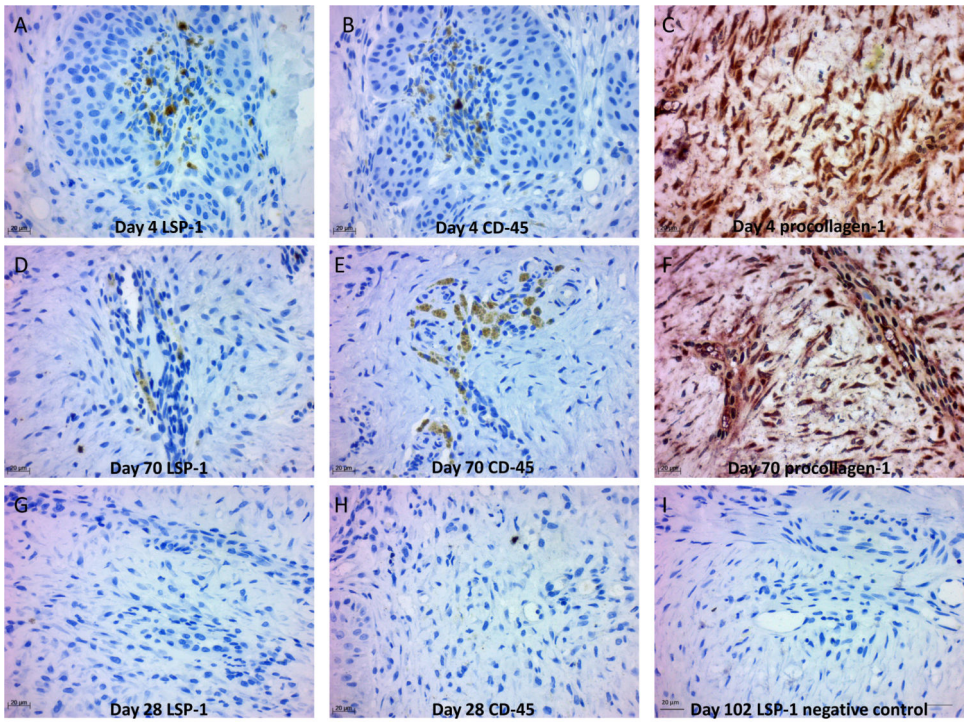

Figure 5.

Photomicrographs of formalin-fixed biopsy specimens at day 4 (A, B, C) and day 70 (D, E, F) after wounding. Immunohistochemical staining is shown for A) LSP-1 day 4, B) CD-45 day 4, C) procollagen-1 day 4, D) LSP-1 day 70, E) CD-45 day 70, and F) procollagen-1 day 70. Biopsies taken at day 28 (G, H) and stained for LSP-1 (G) and CD-45 (H) showed no staining. Procollagen-1 was still present at this time point (data not shown). Control biopsies showed no staining. A representative LSP-1 control image from day 102 is shown in image I. 100x magnification.

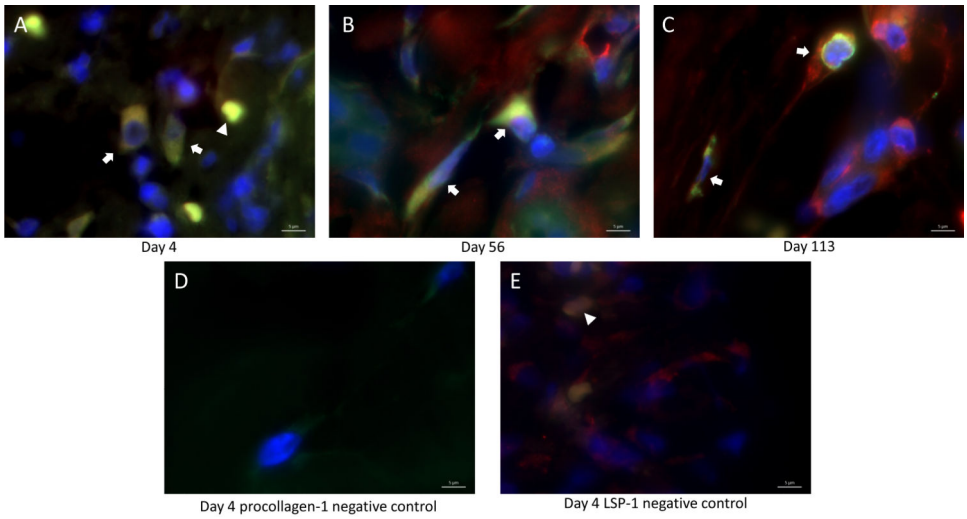

Figure 6.

Photomicrographs of formalin-fixed biopsy specimens at day 4 (A, D, E), day 56 (B), and day 113 (C) after wounding. Immunofluorescent staining for LSP-1 (green) and procollagen-1 (red) with DAPI counterstain (blue) is shown with the colocalization of LSP-1 and procollagen-1 leading to a yellow color indicating the presence of fibrocytes (A, B, C). Control samples from day 4 lacked either procollagen-1 (D) or LSP-1 (E) primary antibody. Fibrocytes with positive colocalization are indicated with arrows. Autofluorescent red blood cells are indicated with arrowheads. 1000x magnification.

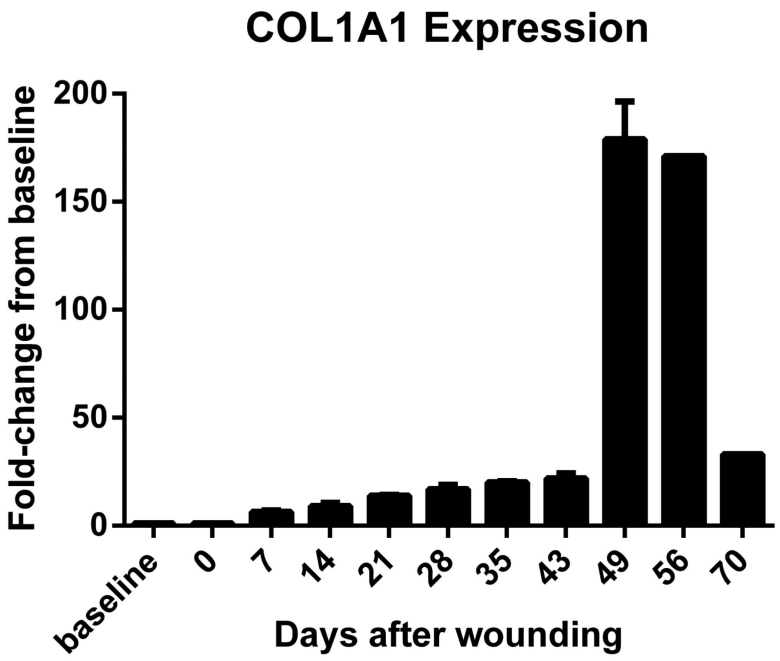

Figure 7.

Graphical representation of COL1A1 expression as fold-change compared to baseline biopsies taken prior to wounding. Baseline level of expression is set at 1. Error bars represent standard deviation from the mean. No error bars are present for days 56 and 70 because only one biopsy for each time point was available for mRNA isolation.

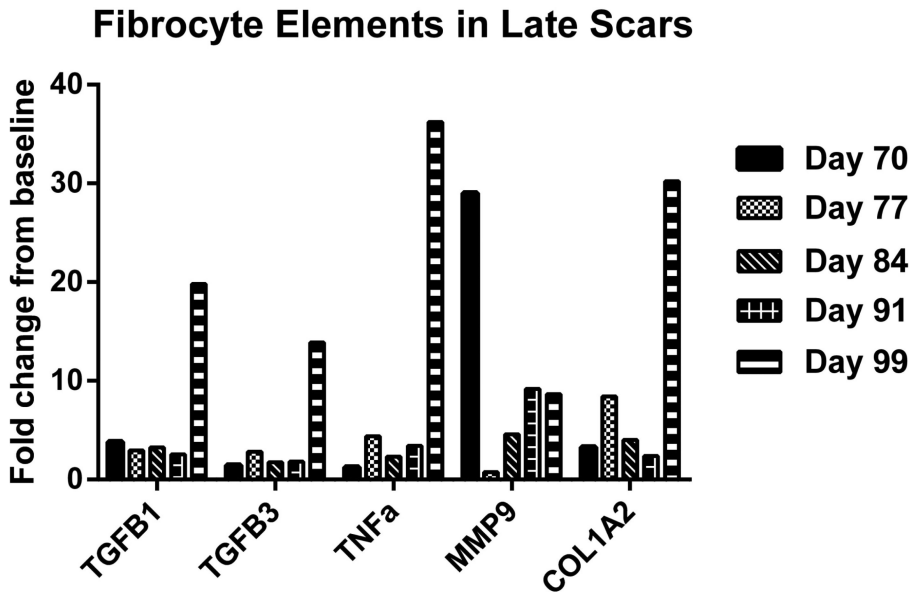

Figure 8.

Graphical representation of TGFB1, TGFB3, TNFα, MMP9, and COL1A2 expression in a subset of late scar samples shown as fold-change compared to baseline biopsies taken prior to wounding.